Supporting Information

Ligand-mediated interfacial engineering in nanocluster-based photo-Fenton-like catalysts: Unveiling the paradox of dispersion versus active site accessibility

Ying Yang*, Fengyu Qian, Xinyu Li, Zirong Tang, Qingnan Meng, Shan Ding, Pan Pan, Lirui Shen, Ju Wu*, Wengui Chang*

College of Materials and Chemical Engineering, Anhui Province Key Laboratory of Conservation and Utilization for Dabie Mountain Special Bio-Resources, West Anhui University, Lu'an, Anhui 237012, P. R. China

Experimental Section

Chemical Reagents. Potassium permanganate ($KMnO_4$, 99%), manganese sulfate ($MnSO_4$) and toluene were supplied by Sinopharm Chemical Reagent Co. Ltd.. Ethanol (EtOH, ≥99.7%), dimethyl sulfoxide (DMSO, ≥99.7%), potassium peroxymonosulfate (PMS, ≥98%), 5,5-dimethyl-1-pyrroline-N-oxide (DMPO, 98%) and 2,2,6,6-tetramethylpiperidine (TEMP, 98%), 2,2,6,6-Tetramethylpiperidine-1-oxyl (TEMPO, 98%), tetracycline hydrochloride (TC, 97%), oxytetracycline hydrochloride (OTC, 95%), methylene blue (MB, 95%), methyl orange (MO, 95%), crystal violet (CV, 95%), rhodamine B (RhB, 95%), p-benzoquinone (BQ, 99%), sodium oxalate ($Na_2C_2O_4$, 99%), furfuryl alcohol (FFA, 99%), tert-butyl alcohol (TBA) and methanol (MeOH, ≥99.7%) were supplied by Shanghai Titan Scientific Co., Ltd. (Adamas, Shanghai, China). All the reagents were used without further purification. The deionized water used throughout all of the experiments was purified through the unique system (resistivity: 18.2 MΩ·cm).

Materials Synthesis. The synthesis of $Au_{25}(SR)_{18}$ nanoclusters (-SR = Capt, PET) was performed following the previously reported method.[1, 2] To synthesize the $Au_{25}(Capt)_{18}$ loaded rod-shaped MnO_2 (thereafter denoted as AuC/MnO_2) and the $Au_{25}(PET)_{18}$ loaded rod-shaped MnO_2 (thereafter denoted as AuP/MnO_2) composite materials, a stir impregnation method after solvent thermal method is conducted. 1.125 g of $MnSO_4$ and 0.7 g of $KMnO_4$ were added into 80 mL of deionized water and vigorously stirred at room temperature for 10 min to form a uniform suspension. Subsequently, the resulting suspension was transferred into two 50 mL autoclaves

(with teflon liners) and reacted at 160°C for 12 h. Finally, the sample was collected via centrifugation and washed by deionized water and ethanol in cycles. The precipitate was collected and dried in an oven at 80°C for 24 h to obtain rod-like MnO_2. Then, 0.5 g of MnO_2 was ultrasonically dispersed in 20 mL of deionized water under vigorous magnetic stirring. Concurrently, 5 mg of $Au_{25}(Capt)_{18}$ dissolved in 8 mL of deionized water was slowly added dropwise to the MnO_2 suspension while maintaining continuous agitation. After aging the mixture for 4 h, the resulting AuC/MnO_2 composite suspension was collected via centrifugation and subsequently subjected to freeze-drying. The synthesis steps for AuP/MnO_2 were similar to AuC/MnO_2, except that the solvent was replaced with toluene and the drying method was changed to rotary evaporation.

Characterization. The sample morphologies were characterized utilizing field-emission scanning electron microscopy (FE-SEM, Hitachi SU8010) and high-angle annular dark-field scanning transmission electron microscopy (HAADF-STEM, FEI-Talos F200X). Phase composition analysis was performed through powder X-ray diffraction (PXRD) on a TD-3700 diffractometer. Ultraviolet-visible (UV-Vis) absorption and diffuse reflectance spectra (DRS) in the 190-900 nm range were acquired with a TU-1950 spectrophotometer coupled with an IS19-2 integrating sphere. Surface elemental composition was examined by X-ray photoelectron spectroscopy (XPS) on a Thermo Fisher ESCALAB250 system. The Brunauer-Emmett-Teller (BET) surface areas were determined using N_2 adsorption-desorption isotherms measured at 77 K with a Micromeritics ASAP 2460 analyzer. The contact angel data were collected by a

JCY-4 measuring device (Fangrui Instrument). Electrochemical analyses were performed in a standard three-electrode configuration using a CHI660E workstation. Photocatalytic experiments employed a 500 W xenon arc lamp (CEL-S500/350) as solar simulator. Electron paramagnetic resonance (EPR) measurements for radical detection were conducted on a Bruker A300 instrument. The quantification of metal in sample was executed by inductively coupled plasma optical emission spectrometry (ICP-OES, Agilent iCAP PRO X Duo).

Photo-Fenton-like catalytic activity test. TC was chosen as model pollutant to evaluate the catalytic activity of nanocatalysts. The standard curves (pollutant concentration vs absorbance) could be seen in Figs. S1-S2 and related literature.[3] The 30 mg of nanocatalysts (MnO_2, AuC/MnO_2 and AuP/MnO_2) were firstly added into TC solution (60 mg/L, 50 mL) and stirred about 60 min to attain adsorption-desorption equilibrium, respectively. In Fenton-like catalytic activity test, PMS (20 mg) and nanocatalysts (30 mg) were simultaneously added to the TC solution (60 mg/L, 50 mL) to initiate the Fenton-like reaction. In photo catalytic activity test, at the same time as the nanocatalysts (30 mg) were added, the light was turned on. In photo-Fenton-like catalytic activity test, PMS (20 mg) and nanocatalysts (30 mg) were simultaneously added to the TC solution (60 mg/L, 50 mL) while the light was turned on. TC degradation was monitored by measuring the absorbance at a wavelength of 356 nm at regular intervals. Different conditions were studied such as catalyst concentration (0.6-3.0 g/L), PMS concentration (0.4-1.6 g/L), temperature (30-60°C) and various pollutant types (TC, OTC, RhB, CV, MB, MO) and concentration (60-120 mg/L). The

degradation efficiency (η, %) and pseudo-first-order reaction rate constants (k_{obs}, min^{-1}) were calculated by the following formulas.

$$\eta = (1- (C_t/C_0)) \times 100\% \quad (1)$$

$$k_{obs}t = \ln (C_0/C_t) \quad (2)$$

where C_0 ($mg \cdot L^{-1}$) is the initial concentration of pollutant, C_t ($mg \cdot L^{-1}$) is the concentration of pollutant at a specific time during the catalytic reaction and t (min) is the reaction time, respectively.

Theoretical calculations. DFT calculations were performed with the first-principles simulation Cambridge Sequential Total Energy Package (CASTEP) module in Materials Studio software. The exchange-correlation potential was described by the generalized gradient approximation (GGA) with the Perdewe-Burkee-Ernzerhof (PBE) functional. A plane-wave basis set with a cutoff energy of 380 eV was assigned to the potential method. The empirical dispersion correction in Grimme's scheme was employed to consider the van der Waals (vdW) interaction. The Broyden-Fletcher-Goldfarb-Shannon (BFGS) algorithm with a medium quality setting of k-points was used for all the energy minimizations in this work. The geometry optimization convergence tolerances for the energy change, maximum force and maximum displacement were 1×10^{-5} eV/atom, 0.001 eV/Å, and 0.005 Å, respectively. For all the models, a 20 Å vacuum space was set in the z-axis to guarantee full relaxation.

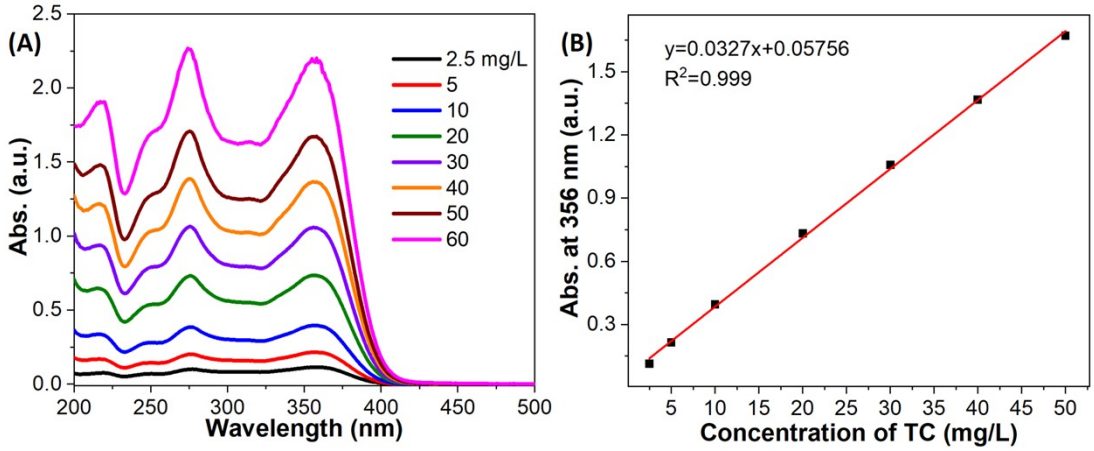

Fig. S1 (A) UV-Vis spectra of TC solution at different concentrations. (B) Standard curve of TC.

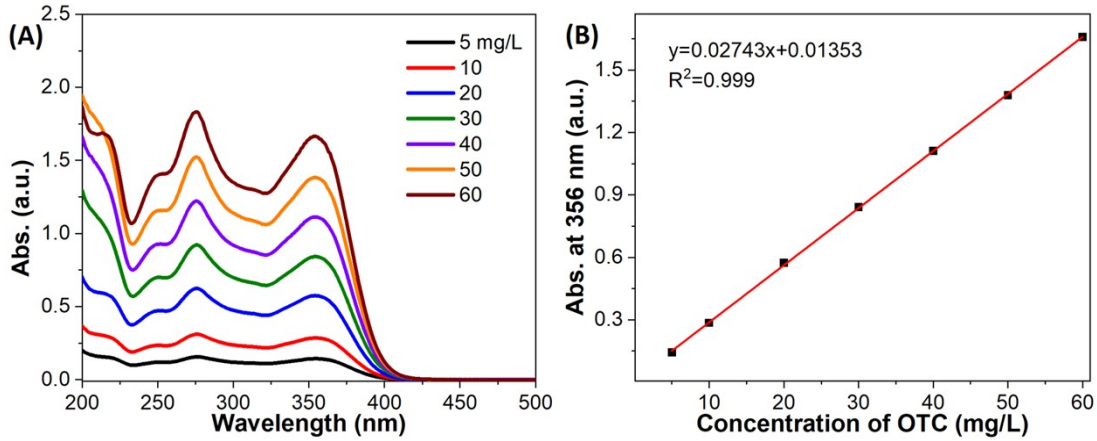

Fig. S2 (A) UV-Vis spectra of OTC solution at different concentrations. (B) Standard curve of OTC.

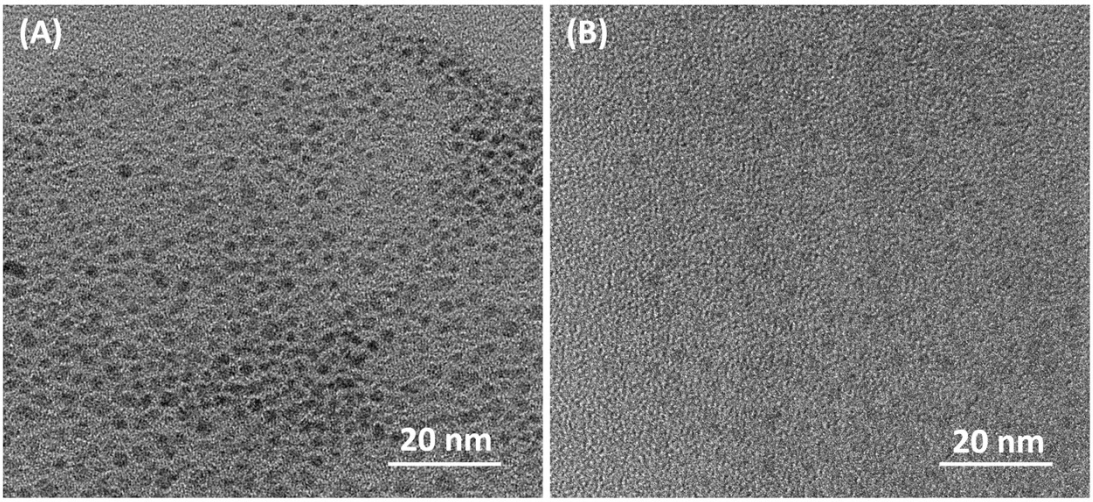

Fig. S3 TEM images of (A) $Au_{25}(Capt)_{18}$ and (B) $Au_{25}(PET)_{18}$.

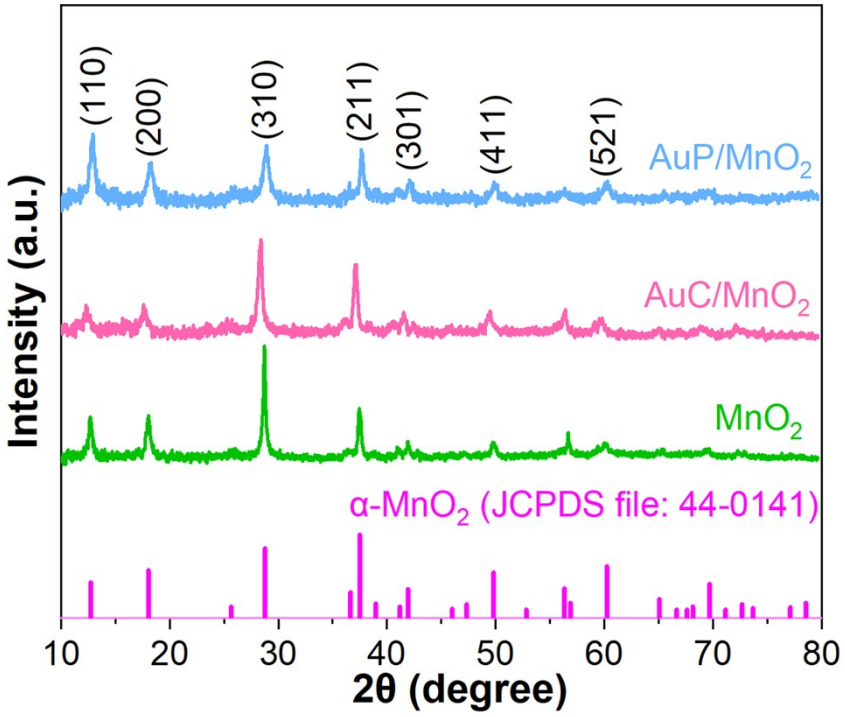

Fig. S4 PXRD spectra of various samples.

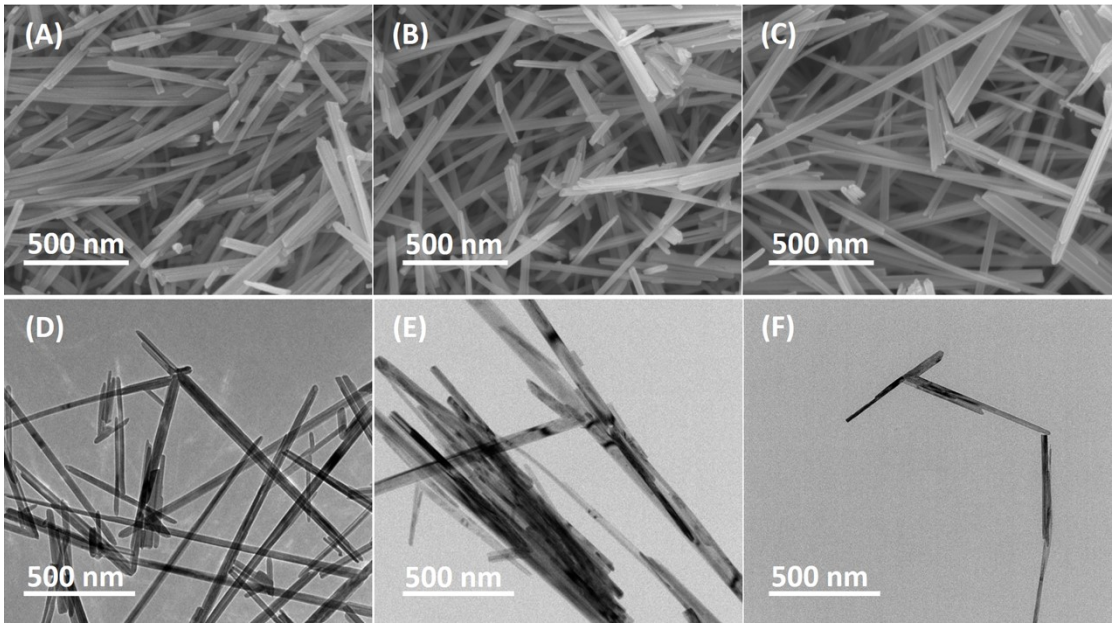

Fig. S5 (A-C) SEM and (D-F) TEM images of (A, D) MnO_2, (B, E) AuC/MnO_2 and (C, F) AuP/MnO_2.

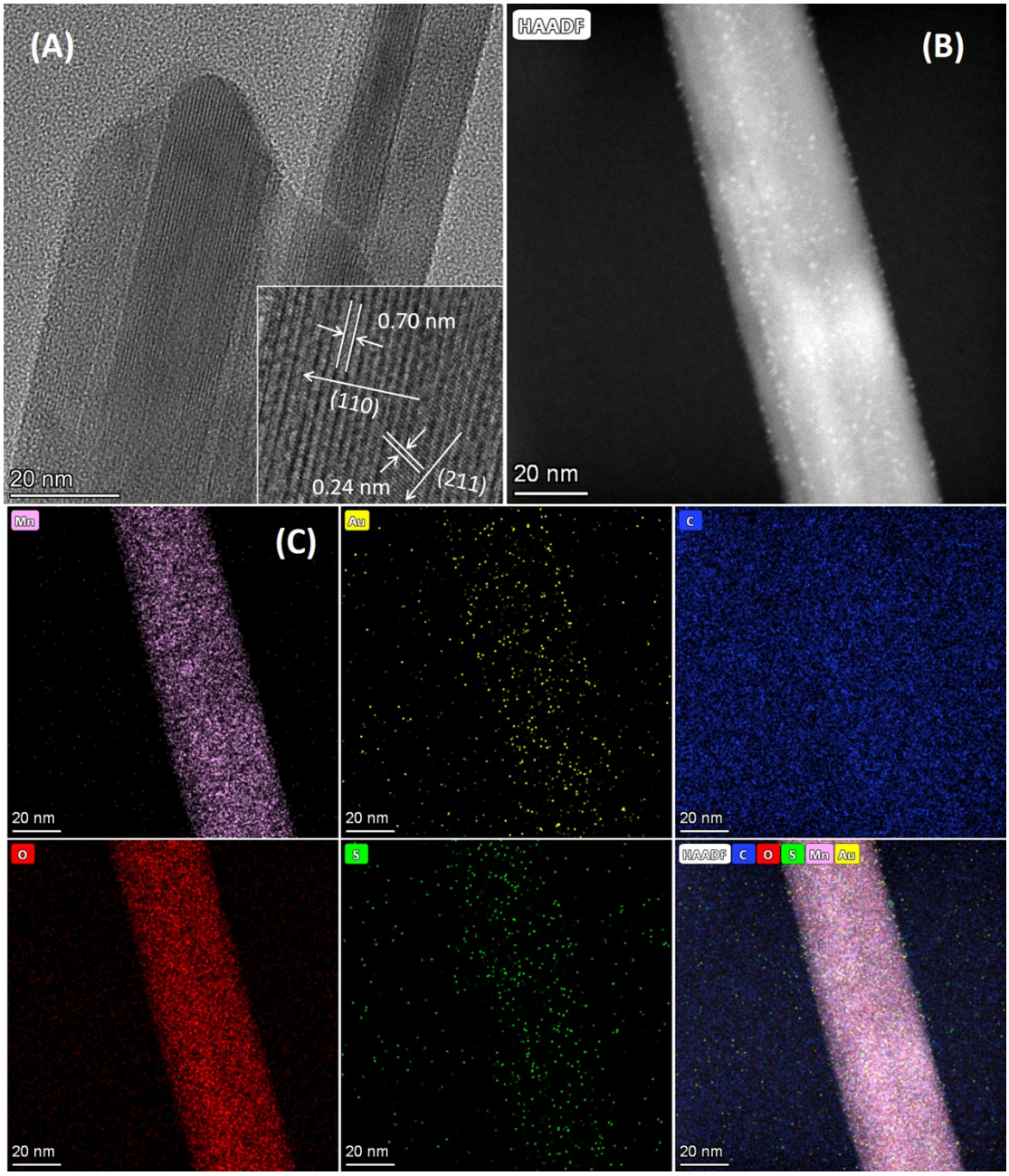

Fig. S6 (A, B) HAADF-STEM images and (C) the corresponding element area distributions of AuC/MnO_2.

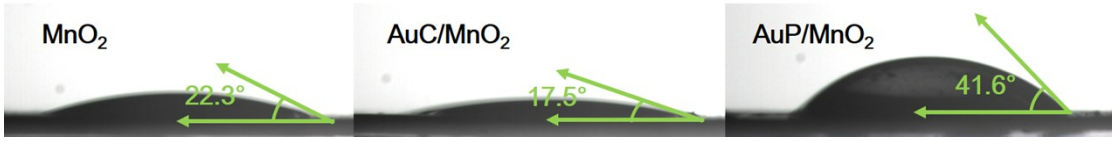

Fig. S7 Contact angels of various samples to de-ionized water.

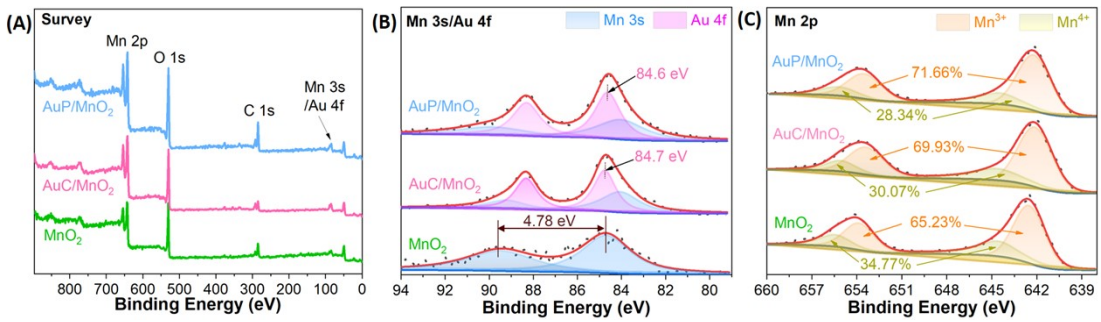

Fig. S8 (A) XPS survey spectra and high-resolution XPS spectra of (B) Mn 3s/Au 4f and (C) Mn 2p.

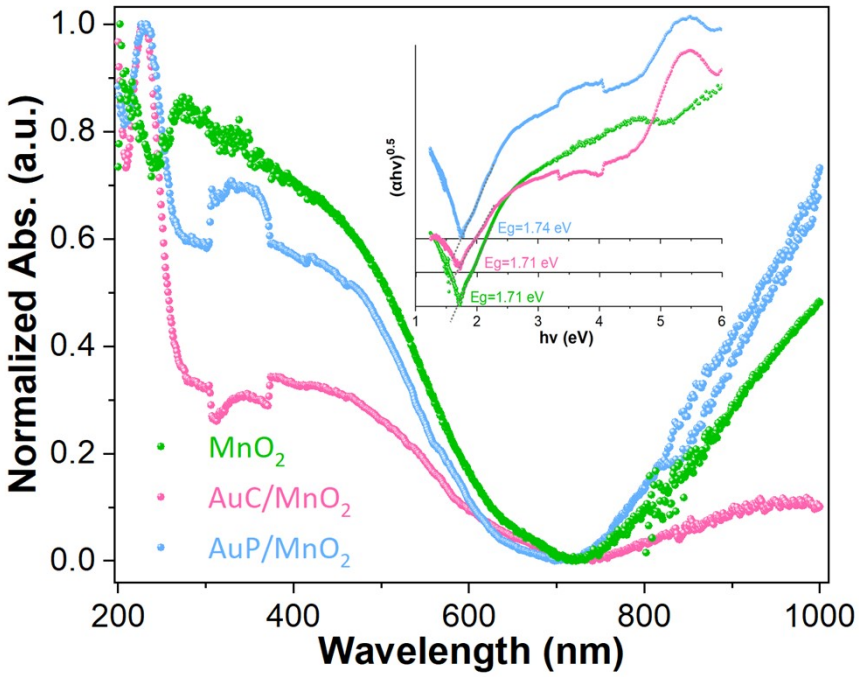

Fig. S9 UV-Vis DRS and Eg of different samples.

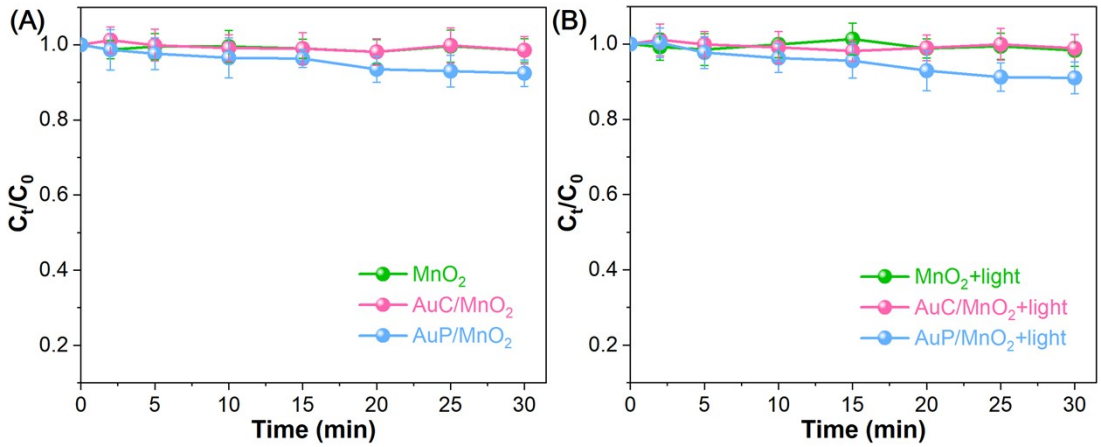

Fig. S10 Comparison of η of TC (60 mg·L^{-1}, 50 mL) under various systems ([catalyst] = 0.6 g·L^{-1}, temperature = 30 ℃, pH = 7±0.2, light power density = 1.0 W/cm^2). The error bars in the figures represent the standard deviations from triplicate tests.

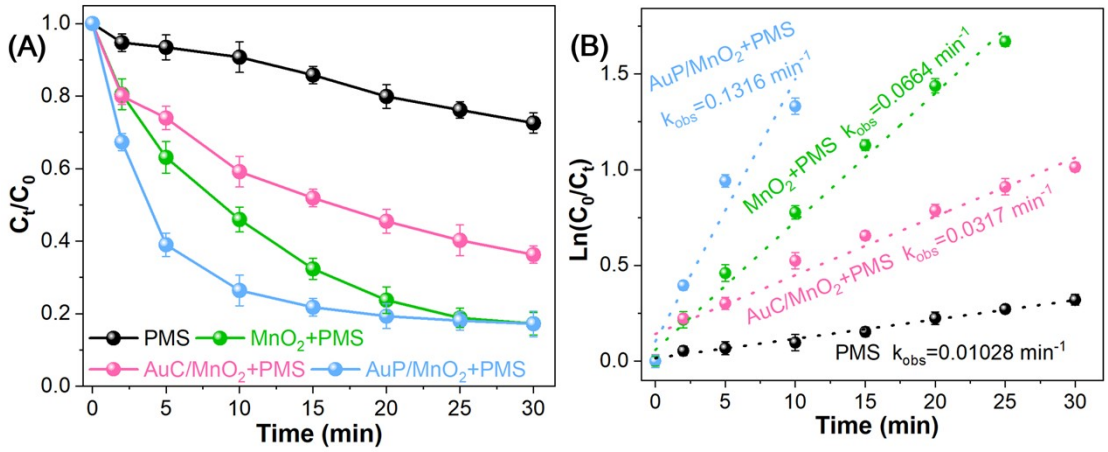

Fig. S11 Comparison of (A) η and (B) k_{obs} of TC (60 mg·L^{-1}, 50 mL) under various systems ([catalyst] = 0.6 g·L^{-1}, [PMS] = 0.4 g·L^{-1}, temperature = 30 ℃, pH = 7±0.2). The error bars in the figures represent the standard deviations from triplicate tests.

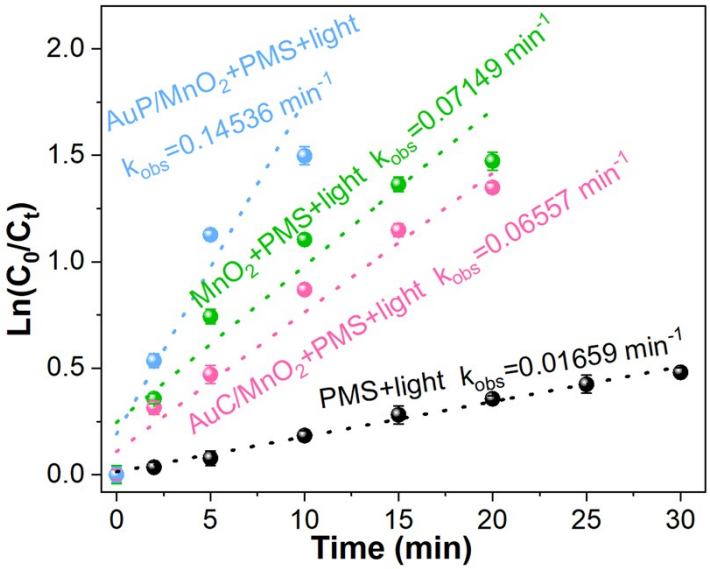

Fig. S12 Comparison of k_{obs} of TC (60 mg·L^{-1}, 50 mL) under various systems ([catalyst] = 0.6 g·L^{-1}, [PMS] = 0.4 g·L^{-1}, temperature = 30 ℃, pH = 7±0.2, light power density = 1 W·cm^{-2}). The error bars in the figures represent the standard deviations from triplicate tests.

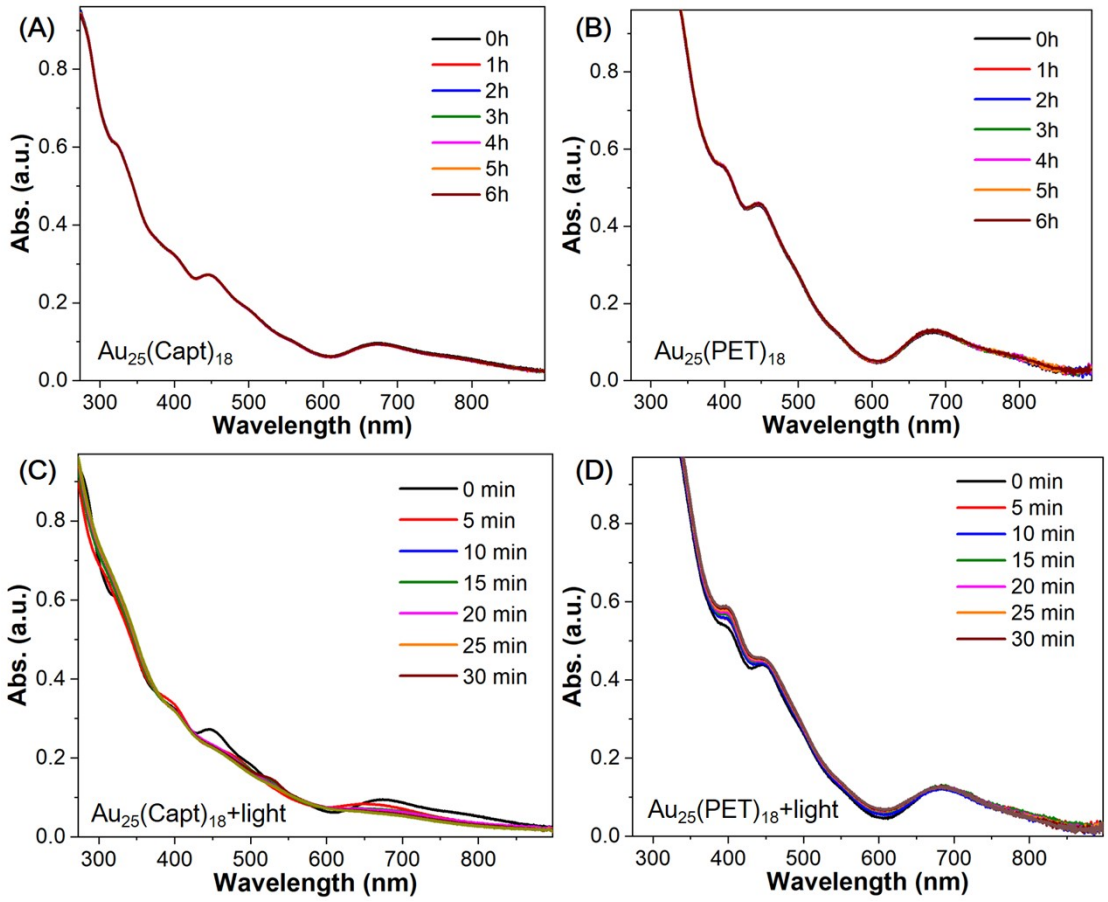

Fig. S13 UV-Vis spectra of $Au_{25}(SR)_{18}$ in water (1 mg·mL^{-1}).

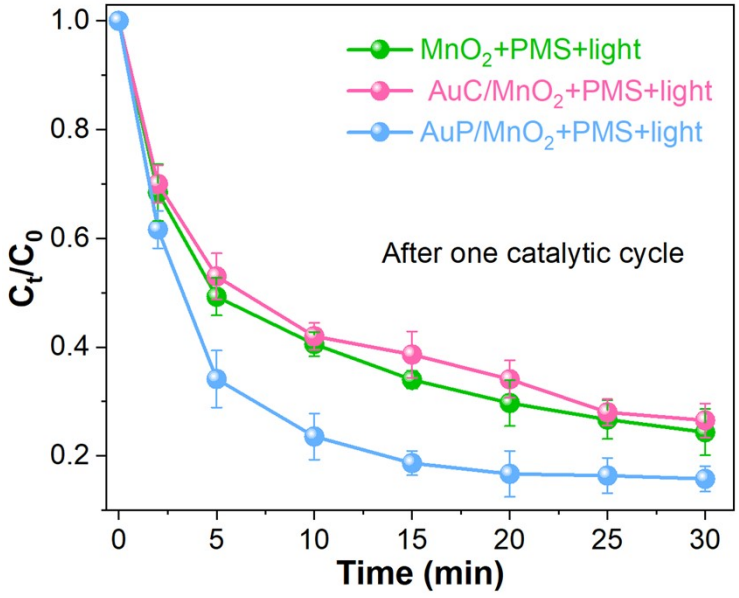

Fig. S14 Comparison of η towards TC (60 mg·L^{-1}, 50 mL) under various systems after one catalytic cycle ([catalyst] = 0.6 g·L^{-1}, [PMS] = 0.4 g·L^{-1}, temperature = 30 ℃, pH = 7±0.2). The error bars in the figures represent the standard deviations from triplicate

tests.

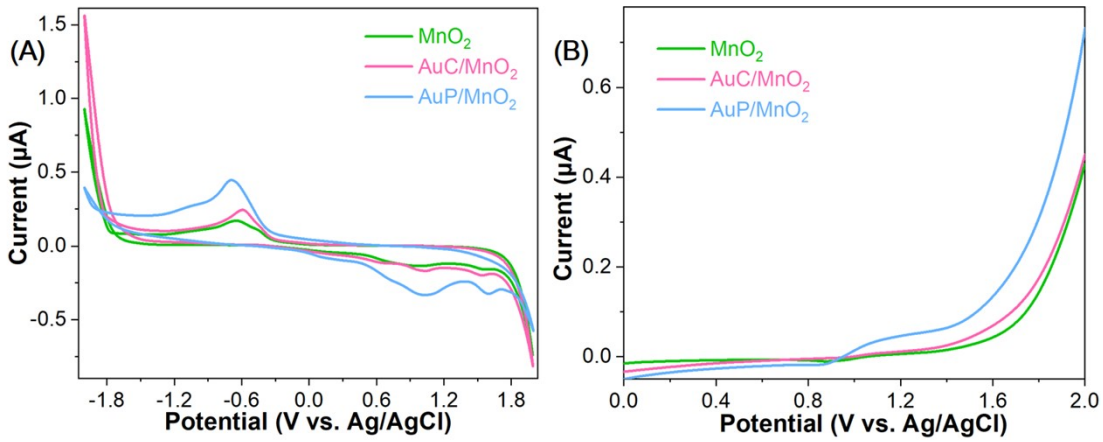

Fig. S15 (A) Linear sweep voltammetry and (B) cyclic voltammetry curves (various nanocatalysts were used as the working electrode at a scan rate of 50 mV/s, 0.05 M Na_2SO_4 solution as electrolyte).

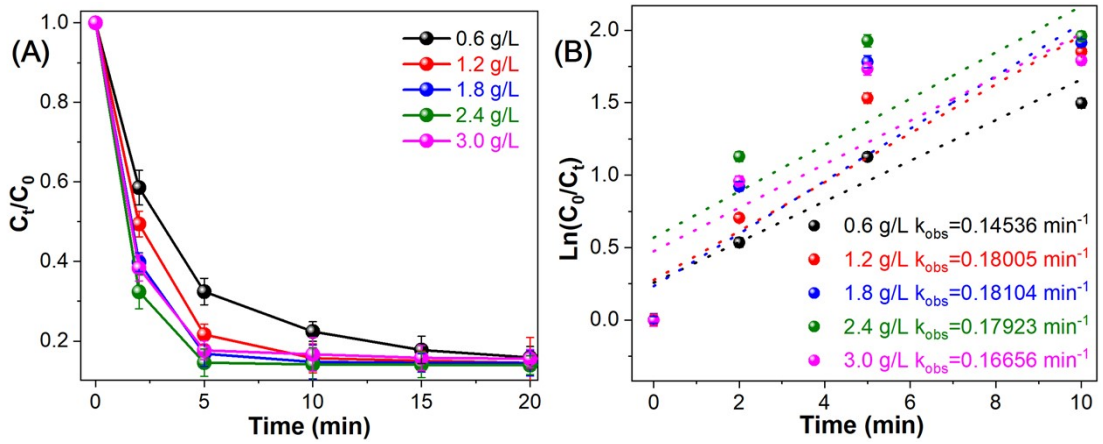

Fig. S16 Effect of AuP/MnO_2 concentration on (A) η and (B) k_{obs} towards TC. [cat.] = 0.6-3.0 g/L, [TC] = 60 mg/L, [PMS] = 0.4 g/L, temperature = 30 ℃, pH = 7±0.2, light power density = 1 W/cm^2. The error bars in the figure represent the standard deviations from triplicate tests.

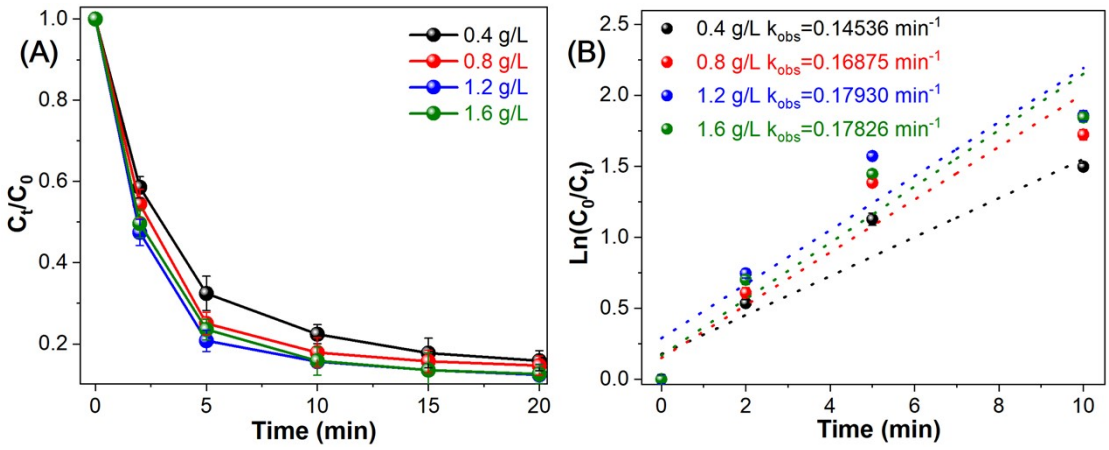

Fig. S17 Effect of PMS concentration on (A) η and (B) k_{obs} towards TC. [cat.] = 0.6 g/L, [TC] = 60 mg/L, [PMS] = 0.4-1.6 g/L, temperature = 30 ℃, pH = 7±0.2, light power density = 1 W/cm^2. The error bars in the figure represent the standard deviations from triplicate tests.

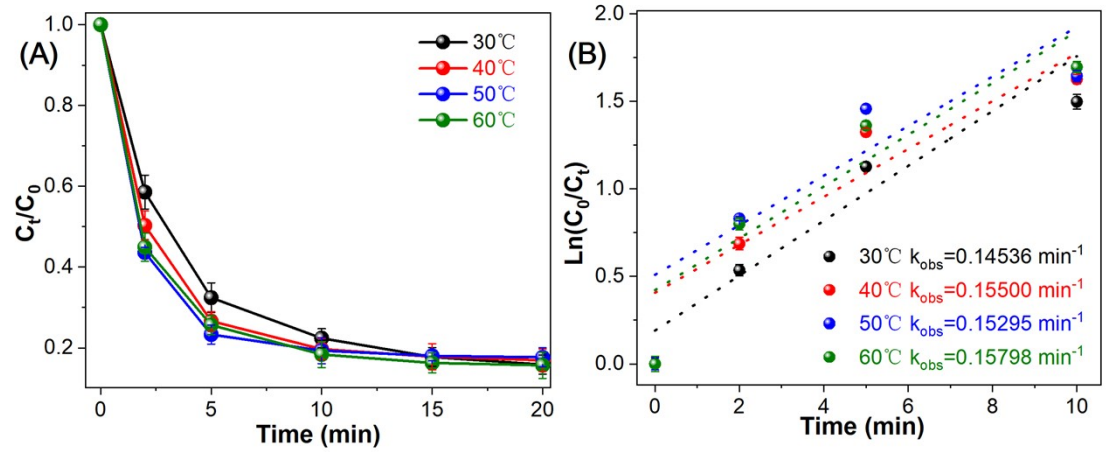

Fig. S18 Effect of temperature on (A) η and (B) k_{obs} towards TC. [cat.] = 0.6 g/L, [TC] = 60 mg/L, [PMS] = 0.4 g/L, temperature = 30-60 ℃, pH = 7±0.2, light power density = 1 W/cm^2. The error bars in the figure represent the standard deviations from triplicate tests.

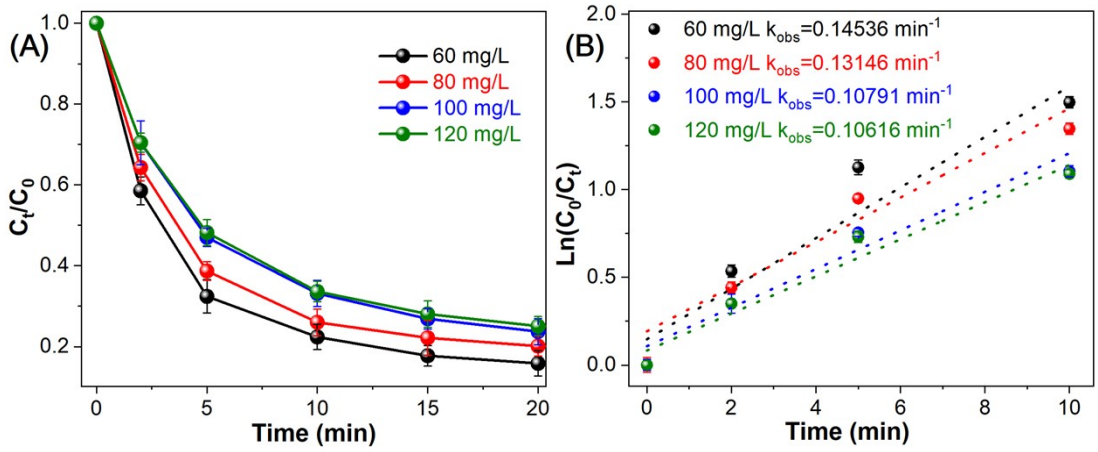

Fig. S19 Effect of TC concentration on (A) η and (B) k_{obs} towards TC. [cat.] = 0.6 g/L, [TC] = 60-120 mg/L, [PMS] = 0.4 g/L, temperature = 30 ℃, pH = 7±0.2, light power density = 1 W/cm^2. The error bars in the figure represent the standard deviations from triplicate tests.

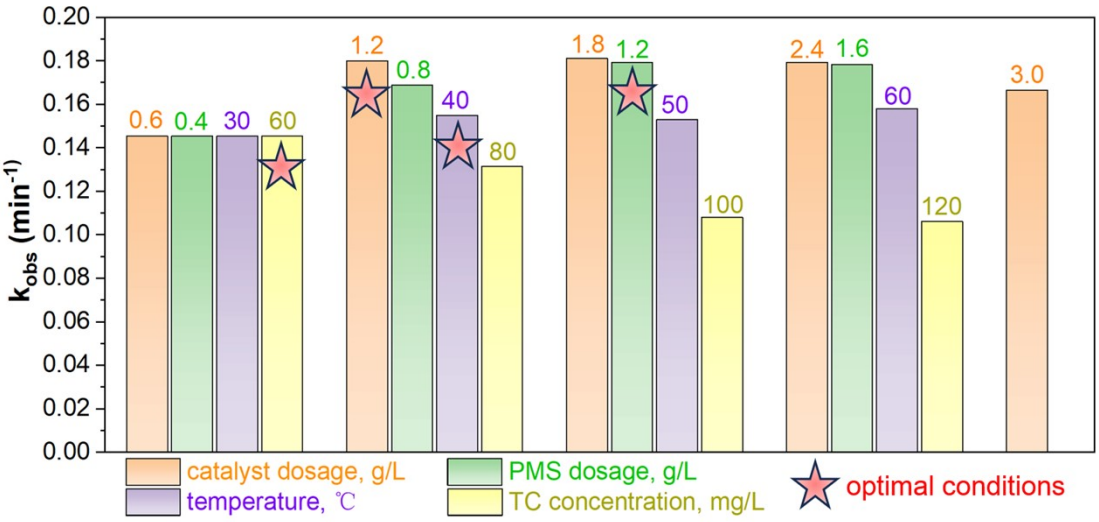

Fig. S20 Influence of catalyst (AuP/MnO_2) dosage, PMS dosage, TC concentration and temperature on k_{obs} values. Optimal conditions: [AuP/MnO_2] = 1.2 g/L, [TC] = 60 mg/L, [PMS] = 1.2 g/L, temperature = 40 ℃, pH = 7±0.2, light power density = 1 W/cm^2.

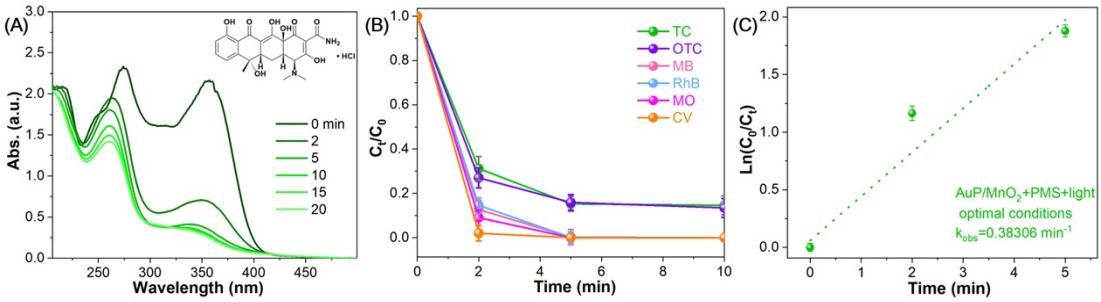

Fig. S21 (A) UV-Vis spectra of degraded TC solution under optimal conditions. (B) Comparison of degradation efficiency of different organic pollutants by AuP/MnO_2 catalysts under optimal conditions. (C) k_{obs} of AuP/MnO_2+PMS system towards TC. The error bars in the figure represent the standard deviations from triplicate tests. Optimal conditions: [cat.] = 1.2 g/L, [TC] = 60 mg/L, [PMS] = 1.2 g/L, temperature = 40 ℃, pH = 7±0.2, light power density = 1 W/cm^2.

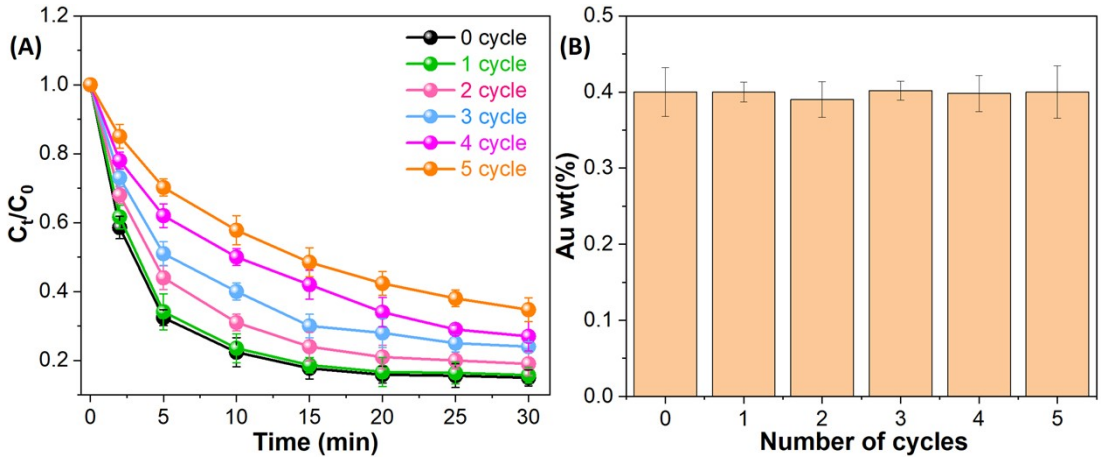

Fig. S22 (A) Comparison of η towards TC (60 mg·L^{-1}, 50 mL) under various systems after five catalytic cycles ([catalyst] = 0.6 g·L^{-1}, [PMS] = 0.4 g·L^{-1}, temperature = 30 ℃, pH = 7±0.2). (B) Au wt% of AuP/MnO_2 after five cycles. The error bars in the figures represent the standard deviations from triplicate tests.

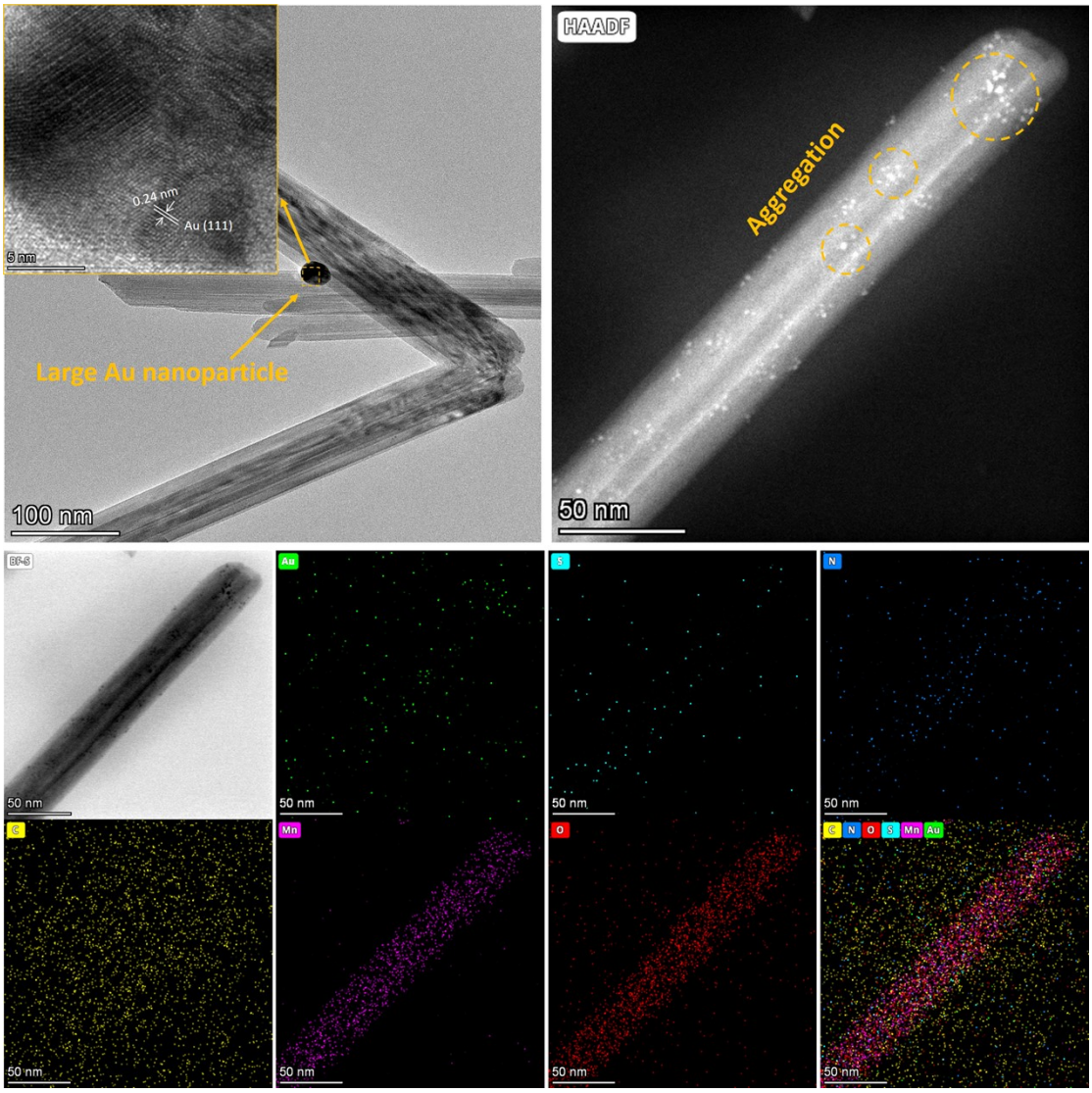

Fig. S23 HAADF-STEM images and the corresponding element area distributions of AuP/MnO_2 after catalytic cycles.

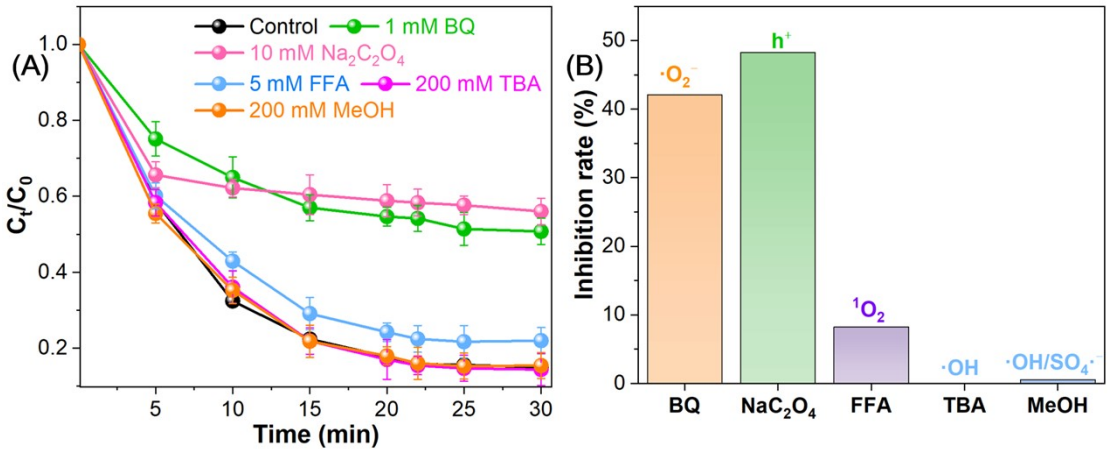

Fig. S24 Effect of active species scavenger on TC (60 mg/L, 50 mL) degradation by the AuP/MnO_2 catalyst (0.6 g/L) + PMS (0.4 g/L) + light (1 W/cm^2) system (temperature = 30 ℃, pH = 7±0.2). The error bars in the figure represent the standard deviations from triplicate tests.

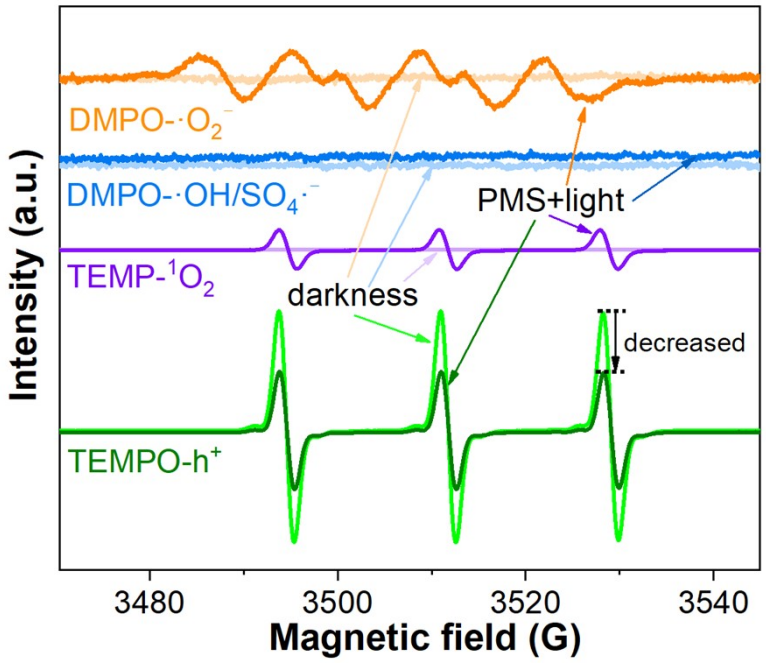

Fig. S25 EPR spectra for the detection of $^{\bullet}OH/SO^{\bullet}_4^-$, $^1O_2$, $^{\bullet}O_2^-$ and h^+ in AuP/MnO_2 system under darkness or PMS+light conditions.

Table S1 ICP-OES results of the contents of Au in the AuC/MnO_2 and AuP/MnO_2.

Name	element	m_0 (g)	V_0 (mL)	C_o (mg/L)	f	C_x (mg/Kg)	wt (%)
AuC/MnO_2	Au	0.0543	100	2.23	1841.6206	4112.807	0.4113
AuP/MnO_2	Au	0.0648	100	2.59	1543.2099	4001.831	0.4002

where m_0 (g) is the mass of catalyst, V_0 (mL) is the constant volume, C_0 (mg/L) is the concentration of solution elements, f is the dilution factor, C_x (mg/Kg) and wt (%) are the element contents of catalyst, respectively.

Table S2 BET surface area, pore diameter and pore volume of different samples.

	Surface parameters		
	BET surface area (m^2/g)	Pore diameter (nm)	Pore volume (cm^3/g)
MnO_2	29.7679	11.6975	0.08157
AuC/MnO_2	23.9290	14.7733	0.07150
AuP/MnO_2	27.1949	12.0154	0.08250

References

1 S. Kumar and R. Jin, *Nanoscale*, 2012, **4**, 4222-4227.

2 M. Zhu, C. M. Aikens, F. J. Hollander, G. C. Schatz and R. Jin, *J. Am. Chem. Soc.*, 2008, **130**, 5883-5885.

3 Y. Yang, F. Qian, Z. Ding, X. Li, C. Dong, C. Shan, X. Liu, P. Li, J. Wu and W. Chang, *Appl. Surf. Sci.*, 2025, **713**, 164319.